

Quantitative investigation of the refractive-index modulation within the core of a fiber Bragg grating

Betty P. Kouskousis, Claire M. Rollinson, Daniel J. Kitcher, Stephen F. Collins and Greg W. Baxter

Optical Technology Research Laboratory, Centre for Telecommunications and Microelectronics, Victoria University,
P.O. Box 14428, Melbourne City MC, Victoria 8001, Australia

Scott A. Wade

Department of Mechanical Engineering, Monash University, P.O. Box 31, Clayton, Victoria 3800, Australia

Nicoleta M. Dragomir and Ann Roberts

School of Physics, University of Melbourne, Victoria 3010, Australia

Abstract: A comparison is made between the modeled and experimentally determined microscopic images of a type I Bragg grating produced in the core of an optical fiber using the ultraviolet irradiation of a phase mask. The simulated image of the refractive-index distribution, which assumes a linear relationship between the irradiation intensity and the refractive-index change, is in good agreement with the measured image.

©2004 Optical Society of America

OCIS codes: (060.2310, 060.2340, 060.2350, 060.2270).

References and links

1. A. Othonos and K. Kalli, *Fiber Bragg gratings: fundamentals and applications in telecommunications and sensing*, (Artech House, Boston, Mass, 1999).
2. R. Kashyap, *Fiber Bragg Gratings*, (Academic Press, San Diego, 1999), Chap. 8.
3. D. Dyer, R. J. Farelly, and R. Giedl, "Analysis of Grating Formation with Excimer Laser Irradiated Phase Masks," *Opt. Commum.* **115**, 327-334 (1995).
4. J. D. Mills, C. W. J. Hillman, B. H. Blott, and W. S. Brocklesby, "Imaging of free-space interference patterns used to manufacture Fiber Bragg Gratings," *Appl. Opt.* **39**, 6128-6135 (2000).
5. C. W. Smelser, S. J. Mihailov, D. Grobnc, P. Lu, R. B. Walker, H. Ding and X. Dai, "Multiple-beam interference patterns in Optical Fiber generated with ultrafast pulses and a phase mask," *Optics Lett.* **29**, 1458-1460, (2004).
6. N. M. Dragomir, C. Rollinson, S. A. Wade, A. J. Stevenson, S. F. Collins, G. W. Baxter, P. M. Farrell and A. Roberts, "Nondestructive Imaging of a Type I Optical Fiber Bragg Grating," *Opt. Lett.* **28**, 789-791 (2003).
7. M. Born and E. Wolf, *Principles of Optics Electromagnetic Theory of Propagation Interference and Diffraction of Light*, 6th ed. (Pergamon Press Ltd, Oxford, 1980), Chap. 8.
8. Charles Kittel, *Introduction to Solid State Physics*, 6th ed. (John Wiley & Sons, New York, 1986), Chap. 2.
9. M. Pluta, *Advanced Light Microscopy: Specialized Methods*, In *Advanced Light Microscopy: Specialized Methods*, M. Pluta (Ed.), 2, (Elsevier, Amsterdam, 1980).
10. K. J. Dana, "Three Dimensional Reconstruction of Tectorial Membrane: An Image Processing Method using Nomarski Differential Interference Contrast Microscopy," Master Thesis, Massachusetts Institute of Technology, Massachusetts, (1992).
11. C. Preza, "Phase Estimation Using Rotational Diversity For Differential Interference Contrast Microscopy," Doctor of Science Dissertation, Sever Institute of Washington University, Saint Louis, Missouri, USA, (2000).
12. N. Dragomir, G. Baxter, P. Farrell, E. Ampem-Lassen and A. Roberts, "Near-Field Measurement of a Wollaston Shear Displacement," *Bienn. Congress AIP*, 331-333, (2002).

1. Introduction

Fiber Bragg gratings (FBGs) have become one of the most widely used components in the fields of optical sensing and telecommunications [1, 2]. Standard FBGs are commonly inscribed by exposing a segment of a single mode photosensitive optical fiber to an ultraviolet (UV) interference pattern created by a phase mask. This exposure induces a periodic refractive-index (RI) modulation in the fiber by modifying the structure of the core material [1, 2].

Much effort has been directed toward analyzing the interference patterns associated with the grating formation [2-6]. Studies of excimer laser irradiated phase masks revealed that the complexity of the intensity distribution varies with the properties of the phase mask [3]. In addition, the Fresnel-Kirchhoff diffraction pattern produced by a phase mask, measured and modeled in free space [4], demonstrated that a Talbot-like diffraction pattern extends out to fill the region of the fiber core during the grating fabrication process. Furthermore, a multiple beam interference model extended to incorporate a time-dependent term, has been demonstrated to adequately describe the cladding patterns for FBG fabrication using picosecond IR pulses together with a phase mask [5].

Differential Interference Contrast (DIC) imaging of a type I FBG fabricated using the phase mask technique verified the existence of a complex structure created in the core of a single mode optical fiber [6]. This detailed structure was consistent with the formation of a three-dimensionally periodic Talbot diffraction pattern [4].

This paper extends the work presented in Ref. [6] to provide a comparison of the structure observed in a DIC image of the Bragg grating with a simulated DIC image predicted by an interference model. The numerical simulation takes into account the properties of the phase mask including writing conditions, the optical properties of the fiber used to fabricate the FBG and the optical properties of the DIC microscope used to image the FBG.

2. Interference pattern formed by a Phase Mask

UV radiation, normally incident on a phase mask, is diffracted to form a three dimensional interference field behind the grating. Ideally, for FBG fabrication, a phase mask having a period of Λ_{pm} , would have diffracted light contained only in the ± 1 diffracted orders forming a set of fringes of period $\Lambda_{pm}/2$ [2]. Consequently, for light travelling through the fiber containing the resulting grating, the resonant Bragg reflection of the incident mode occurs at the wavelength $\lambda_B = 2n_{eff}\Lambda_{pm}$, where n_{eff} is the effective refractive-index of the core.

The diffracted light patterns from standard phase masks however contain contributions from higher diffracted orders; so that the interference pattern formed should be evaluated using Fresnel-Kirchhoff diffraction theory [7]. The contributions from each diffracted component, ignoring vector effects, can be superposed to generate the field, $E(x,y)$ produced by the interference of diffracted beams [8]:

$$E(y, x) = \sum_m C_m \exp(imGy) \exp(ik_m x), \quad (1)$$

where $k_m = (k^2 - m^2 G^2)^{1/2}$, $G = 2\pi/\Lambda_{pm}$, $k = 2\pi/\lambda_{UV}$, m is an integer, λ_{UV} is the wavelength of the incident light, and C_m is the amplitude of the electric field of the m^{th} diffracted order. For this investigation the x -direction denotes the direction of the incident UV beam (i.e. light propagating transversely to the fiber), with the y -axis denoting the grating array direction, (i.e. along the axis of the fiber).

For the purposes of this work, it is assumed that there is a linear relationship between the RI change induced in the glass and the modeled diffracted intensity distribution. The refractive index in the medium behind the grating was taken to be $n = 1.469$.

3. Intensity distribution for a measured differential interference contrast image

The Nomarski DIC imaging system is an interferometric microscope and its principal advantage is that it generates high spatial resolution contrast of a thin optical section of a transparent specimen by exploiting optical path differences within the specimen. This imaging system has been described in detail elsewhere [9, 10, and 11] so only a brief overview is presented here. The image formation in a Nomarski DIC microscope is based on the interference of two light beams. An incoming plane linearly polarized beam is split into two orthogonal components using a Nomarski-modified Wollaston prism. As these beams leave the prism, they are in phase but are spatially separated over a very small distance, commonly referred to as the lateral shear. After passing through the objective lens and the object, each beam is either phase advanced or retarded depending on the object refractive-index and its thickness. The two beams are then recombined by a second Wollaston prism and brought into the same vibrational plane by an analyzer. This way refractive-index changes encountered by either beam will result in different optical paths between them.

Under coherent illumination, the intensity distribution measured in a DIC image is governed by the magnitude of the convolution of the point spread function (PSF), $h(x, y)$, of the optical system and the complex object transmission function, $f(x_0, y_0)$ [11]:

$$I(x,y) = \frac{a}{\lambda f_{con}} \left| \int_{-\infty}^{+\infty} \int_{-\infty}^{+\infty} f(x_0, y_0) h(x - x_0, y - y_0) dx_0 dy_0 \right|^2, \quad (2)$$

where a is the intensity of the light at points inside the condenser aperture lens, (x_0, y_0) and (x, y) are points in the object and image plane respectively, f_{con} is the focal length of the condenser lens and λ is the wavelength of the source

4. Optical fiber parameters

The FBG was fabricated in standard telecommunications fiber with a full-width half-maximum (FWHM) core diameter of approximately 8 μm ; details of the transmission characteristics of the FBG can be found in Ref. [6]. The amplitude of the RI profile of the fiber used was measured using a York S14 fiber RI profiler at Laboratoire de Physique de la Matière Condensée, (LPMC) Nice, France and is shown in Fig. 1. It can be seen in Fig. 1. that there is a refractive index mismatch between the fiber cladding ($\pm 60 \mu\text{m}$) and the index matching fluid used in the measured refractive index profile, (dotted line).

A super-Gaussian function (also referred to as a top-hat function), characterized by a flat distribution and steep edges was generated using the measured RI amplitude to best fit the edges of the fiber in the measured DIC image [6], shown in Fig. 1., (solid line) The super-Gaussian function is given by

$$I(r) = I_0 e^{-2\left(\frac{r}{w}\right)^n}, \quad \text{with } n > 2 \quad (3)$$

where I_0 is the peak amplitude, w is the radius of the mode, and n is the super-Gaussian order.

For this investigation, a super-Gaussian (order 6) was used to best fit the edges of the fiber with a mode diameter, $2w$, of 9 μm . The refractive-index of the core and cladding of the optical fiber were taken as 1.469 and 1.464 respectively.

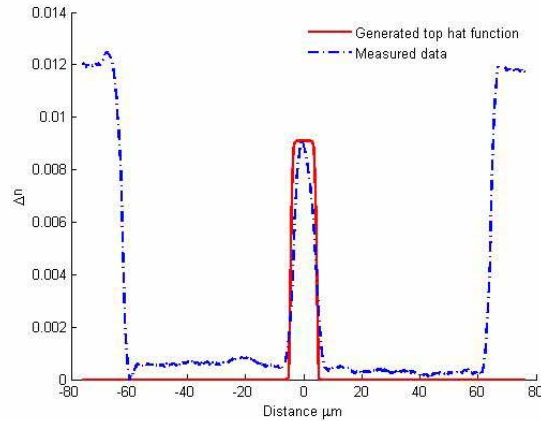


Fig. 1. Refractive-index profile of a single mode optical fiber. The measured data (dotted line) is fitted with a top hat profile (solid line) generated from the measured RI for the purpose of this work.

5. Analysis of the diffracted distribution intensity

The FBG imaged in Ref. [6] was fabricated using an UV continuous wave frequency-doubled Argon ion laser operating at an output power of 106 mW, a wavelength of 244 nm and a beam divergence of 1 mrad. The phase mask, (LasirisTM) having a period of 1.059 μm , was designed to suppress the zeroth diffracted order, with a nominal contribution of less than 3% in the zeroth and approximately 38% in the ± 1 diffracted orders.

In the absence of a fiber, the diffraction efficiencies were measured in the far field under 244 nm illumination at normal incidence and are shown in table 1. It was assumed that 0.1% of the incident power was lost due to scattering.

Table 1. Diffracted orders measured in the far field

Diffraction Orders	0	+1	-1	+2	-2	+3	-3	+4	-4
% power (± 0.3)	0.9	39.5	36.7	3.9	4.6	4.1	3.5	3.0	3.7

Table 2. Calculated range across grating in which diffracted orders overlap coherently

Diffraction Orders	Propagating angle (degrees)	Coherence range $z(\mu\text{m})$
1	9.02°	523
2	18.26°	252
3	28.05°	156
4	38.81°	103

Table 2 shows the propagating angles for the measured diffracted orders produced by the phase mask in a medium of refractive-index 1.469. In addition, it provides the distance over which the diffracted orders overlap coherently, z ,

In this analysis, it was assumed that the fiber core was placed approximately 100 μm away from the phase mask. Under such conditions and using table 2, the diffracted orders considered in this investigation includes those up to ± 2 since the contributions from other orders would be incoherent within the fiber core.

6. Imaging System Parameters

The DIC image of the FBG in Ref [6], was obtained using an inverted Olympus IX FL infinity-corrected optical system, in conjunction with an Argon-ion laser operating on a single line at 488 nm, where the laser beam was raster scanned by galvo mirrors over an area of the specimen. The PSF of the system was measured experimentally using a near-field optical point light source [12]. In addition, the lateral shear was measured confirming a value of $(0.58 \pm 0.01) \mu\text{m}$.

For the purpose of this work, in order to take into account the finite spatial resolution of the system, the PSF was modeled as a linear superposition of two laterally offset Gaussian beams incorporating other lens imperfections. This approach is consistent with early experimental measurements of the PSF of the imaging properties of our system [12].

7. Results

Applying the measured relative diffraction efficiencies to Eq. (1), the intensity distribution produced in the region that occupies the fiber core was simulated to replicate the intensity distribution produced in the optical fiber core. Using coupled-mode theory, the estimated value of the effective refractive-index change was 1.7×10^{-4} [6]. However, in the work presented here a peak amplitude RI modulation of 6×10^{-4} was applied to the intensity distribution; chosen to match the measured DIC image. The discrepancy in these two values arises from the fact that coupled-mode theory assumes uniform sinusoidal variation along the axis of the fiber. It is evident from the measured DIC image shown in Fig. 2 that the variation along the axis of the fiber is not uniformly sinusoidal.

Defining a region that covered a section of the fiber core and the cladding, the scaled intensity distribution was combined with the generated top hat profile. The phase gradient was determined and convolved with the calculated PSF and applied to Eq. (2) to model the intensity distribution produced at the image plane in a DIC microscope. The measured and simulated DIC images of a type I FBG are shown in Fig. 2.

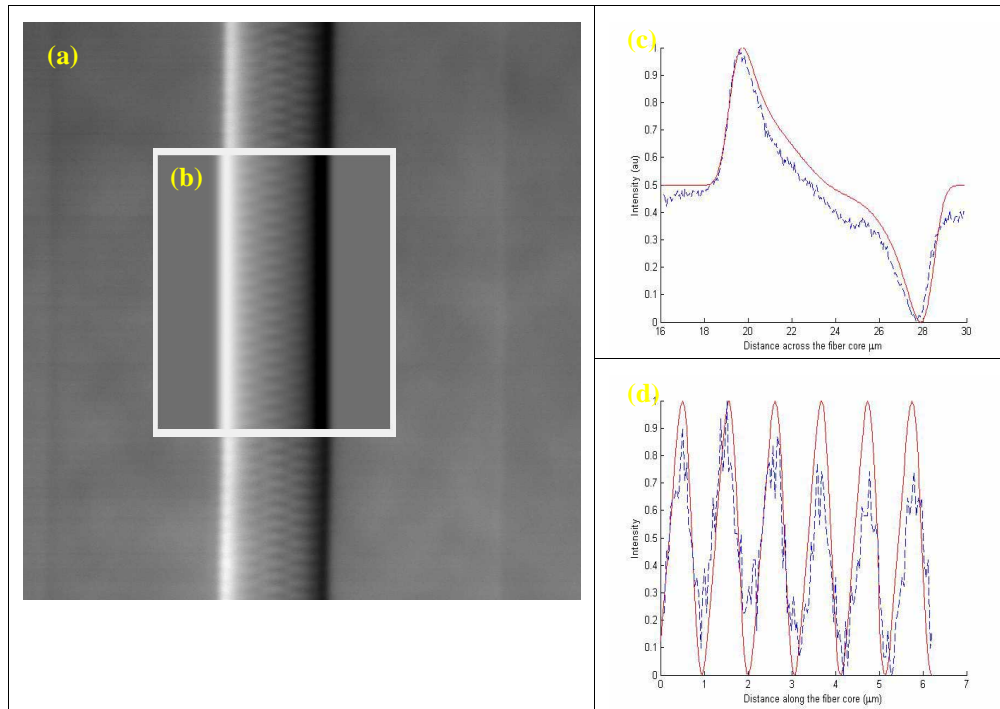


Fig. 2. Left panel: (a) FBG structure written in a single mode fiber with a $1.059 \mu\text{m}$ phase mask. (a) DIC image, $47 \mu\text{m} \times 47 \mu\text{m}$, of the FBG viewed in a direction orthogonal to the UV writing beam. (b) Inset representing DIC numerical simulation of the core region including the FBG structure. Right panel: Comparison of profiles through the observed and modeled image: (c) Profiles across the fiber core, observed data (dotted line) and numerical simulation (solid line). (d) Profiles along the fiber core observed data (dotted line) and numerical simulation (solid line)

Figure 2 shows the simulated image inserted onto the measured DIC image. The simulated image shows features of artificial three-dimensional relief shading that is characteristic of the DIC technique. The bright vertical band to the left of the centre identifies one edge of the fiber core and the black vertical line identifies the other edge.

The two images appear to be similar and show a distance of approximately $8 \mu\text{m}$ between the fiber edges, [Fig. 2 (c)]. The observed discrepancy between the measured and simulated data may be attributed to several differences between the actual imaging conditions and the ones assumed in the generation of the simulated data. Additionally there may be small errors in the bias and shear value and direction, causing errors in the computation of the system's PSF.

The periodicity in the simulated DIC image was evaluated across and along the fiber core for various positions and was found to be $4.5 \pm 0.1 \mu\text{m}$ across the fiber core. This value is in agreement with the value in the measured image of $4.8 \pm 0.2 \mu\text{m}$. Along the fiber core, a dual periodicity of $1.058 \pm 0.02 \mu\text{m}$ and $0.506 \pm 0.02 \mu\text{m}$ was found, [Fig. 2(d)] which agrees well with the results reported in Ref. [6].

8. Conclusion

A direct relationship between the effects of higher orders produced by a phase mask and the non-circularly symmetric refractive-index features within a FBG, measured using the DIC microscopy technique have been established by this work. The strongest characteristics of the image have been shown to result from the beating between the 1st and 2nd diffraction orders of the phase mask.

Further work, studying the structure of type II and type IIA gratings together with modeling of the reflection and transmission spectra arising from these complex structures is continuing.

Acknowledgments

The authors gratefully acknowledge the financial support of the Australian Research Council and the software assistance of Dr. John Roumeliotis of Victoria University. G. W. Baxter's e-mail address is gregory.baxter@vu.edu.au.